Silver nanoparticles induce a 'triclosan like' antibacterial action mechanism in multi-drug resistant *Klebsiella pneumoniae*

Vikram Pareek[1,2], Stéphanie Devineau[3], Sathesh K. Sivasankaran[4], Arpit Bhargava[2], Jitendra Panwar[2]*, Shabarinath Srikumar[5] and Séamus Fanning[1,6]*

[1] UCD-Centre for Food Safety, UCD School of Public Health, Physiotherapy and Sports Science, University College Dublin, Dublin D04 V1W8, Ireland
[2] Department of Biological Sciences, Birla Institute of Technology & Science, Pilani 333031, India
[3] Université de Paris, BFA, UMR 8251, CNRS, F-75013 Paris, France
[4] Genome Informatics Facility, Iowa State University, 448 Bessy Hall, Ames, IA, 50011, USA
[5] Department of Food, Nutrition and Health, College of Food and Agriculture, UAE University, Al Ain, UAE
[6] Institute for Global Food Security, Queen's University Belfast, 19 Chlorine Gardens, Belfast BT9 5DL, United Kingdom

Corresponding authors:
* Jitendra Panwar (jpanwar@pilani.bits-pilani.ac.in)
* Séamus Fanning (sfanning@ucd.ie)

Abstract

Infections associated with antimicrobial-resistant (AMR) bacteria now represent a significant threat to human health using conventional therapy. Since AMR bacterial infections are poised to overtake cancer as the main cause of death by 2050, scientists are exploring the efficacy of novel antimicrobial strategies, such as use of silver nanoparticles (Ag NPs) to combat infections. Whilst Ag NPs may hold therapeutic promise, their mode of action on the bacteria remains to be elucidated. In this study, lysozyme coated Ag NPs were synthesized and characterized by TEM-EDS, XRD, UV-vis, FTIR spectroscopy, zeta potential and oxidative potential assay. Ag NPs with an average diameter of 5.2 ± 1.2 nm were found to be bactericidal against multi-drug resistant *Klebsiella pneumoniae* MGH78578. Deep level transcriptional analysis using RNA sequencing revealed that Ag NPs induced a triclosan-like bactericidal mechanism. RNAseq data showed that Ag NPs were responsible for the inhibition of the type II fatty acid biosynthesis. Additionally, released Ag^+ generated oxidative stress both extra- and intracellularly in *K. pneumoniae*. We show that triclosan-like activity and oxidative stress cumulatively underpinned the antibacterial activity of Ag NPs. This result was confirmed by the analysis of the bactericidal effect of Ag NPs against the isogenic *K. pneumoniae* MGH78578 *ΔsoxS* mutant, which exhibits a compromised oxidative stress response compared to the wild type. Here we provide evidence to extend our understanding of the

anti-*Klebsiella* activity associated with silver nanoparticles. This allowed us to model how bacteria might develop resistance against silver nanoparticles, should the latter be used in therapy.

Significance Statement

Many pathogens including *Klebsiella pneumoniae* have evolved to become resistance to antimicrobial agents, necessitating the development of alternate and more effective antibacterial compounds. Silver nanoparticles have been proposed as potential antimicrobial agents. However, a complete understanding of the antimicrobial activity of silver nanoparticles is required before these molecules can be used in therapy. Here, we used biochemical assays and RNA sequencing to decipher how silver nanoparticles exert their antibacterial action against multi-drug resistant *K. pneumoniae* MGH78578. We observed that silver nanoparticles behave similarly with another antimicrobial agent, triclosan. This unique observation provides some clues about how bacteria respond to exposure with silver nanoparticles.

Keywords: Silver nanoparticles; *Klebsiella pneumoniae*; RNA sequencing; soxS; triclosan.

Introduction

Antimicrobial agents were once heralded as 'magic bullets' due to their utility for the treatment of infectious disease. However, the indiscriminate use of these compounds contributed to the emergence of antimicrobial resistance (AMR) in pathogenic bacteria. Currently, humanity is headed back to a pre-antibiotic era where even minor infections can prove untreatable and fatal (1). Antimicrobial resistance is responsible for approximately 700,000 deaths annually across the globe and this number is expected to increase further if new measures are not adopted and antibacterial compounds discovered (2). The emergence of MDR in various pathogenic bacterial species represents a serious public health challenge, leading to hospital- and community-acquired infections, which are difficult to treat and control (3, 4). Since AMR is estimated to overtake cancer as the main cause of death in 50 years, innovative approaches including the development of novel antimicrobial strategies using silver nanoparticles (Ag NPs) are required.

Klebsiella pneumoniae is one of the members of the ESKAPE pathogens (representing *Enterococcus faecium, Staphylococcus aureus, Klebsiella pneumoniae, Acinetobacter baumannii, Pseudomonas aeruginosa* and *Enterobacter* spp.) (3). It is a member of Enterobacteriaceae family - Gram-negative, non-motile, and rod-shaped. This bacterium is considered an opportunistic pathogen commonly found in the intestine, mouth, and skin of humans. It is mainly associated with hospital-acquired infections (nosocomial infections) and responsible for respiratory/urinary tract infections (UTI), pneumonia, and sepsis (2, 5, 6). This pathogen can also form biofilms on indwelling medical devices leading to persistent nosocomial infection (7, 8). The mechanism associated with its bacterial pathogenicity has been reviewed by Li *et al* (8) and Hu *et al* (9).

About 25 % of nosocomial *K. pneumoniae* were found to be resistant to carbapenem-based compounds (10). Further, *K. pneumoniae* were also found to be resistant to colistin, a last-line antibiotic (11, 12). The emergence of resistance in *K. pneumoniae* against critically important classes of antibiotics represents a major threat to conventional clinical therapy. Therefore, novel antibacterial strategies are required to overcome this challenge (13).

Inorganic metals, including silver, copper, and zinc have historically been used as potential antibacterial agents. Among these, silver is particularly favoured, primarily because of its well-established history of use (14). Antibacterial activity of silver can vary depending on its chemical form (14-16). Metallic forms of silver continuously release small numbers of ions, which makes it a slow-acting agent, whilst the ionic form is more efficient. Although Ag^+ is reported to exhibit better antibacterial activity, direct exposure to mammalian cells has toxic side effects that limit its application in therapy (17). In contrast, the nano form of silver provides a greater surface area to volume ratio in comparison to larger particles, leading to a more controlled and constant release of

Ag^+. Hence, this form has potential as an antibacterial compound. Despite this advantage, little is known about the antibacterial action mechanisms of silver-based nano-antibacterial formulations.

Here, we describe the antibacterial action mechanism associated with silver nanoparticles (Ag NPs) using a multi-drug resistant strain of *K. pneumonia, K. pneumonia* MGH78578, as a model bacterium. Firstly, we synthesized lysozyme coated silver nanoparticles (L-Ag NPs) and characterized them for their antibacterial mechanism against *K. pneumonia* MGH78578. The antibacterial mechanism was analyzed (i) focusing on physiological and biochemical analysis, where we evaluated the membrane damage and oxidation potential in L-Ag NP exposed bacteria, primarily to study the extent of bacterial damage, (ii) using RNA sequencing (RNA-seq), the stress responses following exposure were identified. These data showed that L-Ag NP exposure induces a *triclosan-like* antibacterial effect in multi-drug resistant *K. pneumoniae.* The latter effect along with Ag^+ induced oxidative stress was responsible for the anti-*K. pneumoniae* effect of L-Ag NPs. Our results provide molecular insights into how bacteria might deploy antibacterial strategies to counteract the toxic effects of L-Ag NPs. This allowed us to futuristically model how *K. pneumoniae* might develop resistance against silver nanoparticles should these nanoparticles enter into conventional therapy.

Results and discussion

Synthesis and characterization of L-Ag NPs

Reduction of metal ions is most commonly employed for the preparation of metal-based NPs in solution. This approach is a first choice method for the synthesis of noble metal NPs and involves the reduction of an ionic salt using various reducing agents in the presence of a stabilizing agent (18-20). L-Ag NPs were synthesized by a co-reduction method wherein lysozyme functions both as a reducing- and a stabilizing agent (18). This co-reduction was achieved using heat reflux action at 120 °C, which leads to the coating of lysozyme on Ag NPs. Here lysozyme acts as a capping material, devoid of enzymatic activity (21, 22). We selected L-Ag NPs for this study based on their bactericidal activity against Gram-negative multi-drug resistant *K. pneumoniae* MGH78578.

The synthesis of L-Ag NPs was associated with a gradual color shift from light to dark red corresponding to the appearance of the plasmon peak at 414 nm in the UV-vis spectrum (Figure 1A) (23). TEM was then used to measure the size and shape of L-Ag NPs. The nanoparticles were found to be quasi-spherical in shape with a diameter ranging from 1-10 nm and an average diameter of 5.2 ± 1.2 nm (Figures 1B-C). The X-ray diffraction pattern of L-Ag NPs are characterized by well-defined peaks at 2Θ values of 38.25°, 46.26°, 64.70° and 77.66° corresponding to (111), (200), (220) and (311) planes, respectively. This diffraction pattern is associated to the face-centered cubic lattice structure of crystalline silver as per the JCPDS file 04-0783 (24, 25) (Figure

1D). The composition of L-Ag NPs was confirmed by TEM-EDS. The EDS spectra show an absorbance peak at 3.0 keV characteristic of silver (Figure S1) (25). As the samples for EDS analysis were prepared by drop coating Ag NPs on to a glass slide, additional peaks at 1.76, 1.0, 0.5, and 0.27 keV corresponding to silicon, sodium, oxygen, and carbon, respectively were also observed.

The surface charge of L-Ag NPs in solution was estimated by measuring their zeta potential in water and modified LB (mLB) medium at 37° C. Modified LB medium corresponds to Luria Bertani culture medium devoid of NaCl, which we used to assess the bactericidal effect of L-Ag NPs against *K. pneumoniae*. L-Ag NPs were found to be negatively charged in both conditions with ζ = -38.2 ± 1.6 mV in water and ζ = -24.2 ± 0.9 mV in mLB medium. We used FTIR spectroscopy to examine the surface capping of L-Ag NPs. The 1,632 cm^{-1} peak corresponds to the amide I vibration characteristic of the protein backbone which confirms the presence of lysozyme associated with silver nanoparticles, though its surface coverage could not be determined (Figure 1E) (1, 18).

L-Ag NPs inhibit the proliferation of *K. pneumoniae* MGH78578 at low concentration

Following synthesis and characterization, the antibacterial activity of L-Ag NPs was measured. It is known that bacteriological media components can have an impact on the measured antibacterial activity of silver species (26). In media with high salt content like chloride and phosphate, Ag NPs may aggregate leading to a reduction in the degree to which they associate with bacterial cells (27) and free Ag^+ can precipitate in the form of silver chloride (28, 29), potentially reducing the bactericidal activity of Ag NPs. Here we used modified LB media (mLB) (19) and compared the growth curves of *K. pneumoniae* MGH78578 in mLB media with that of LB media. The comparative analysis did not show any significant difference between the growth of *K. pneumoniae* in mLB and LB (Figure 2A).

Growth curves obtained demonstrated a short lag phase for both LB and mLB. This could be because growing bacterial cells (mid-log phase) were used as the inoculum, and these bacteria adapted quickly. Since there were no phenotypic differences between LB and mLB, the latter was chosen as the bacteriological growth media for further experiments.

Next, the viability of L-Ag NP exposed *K. pneumoniae* MGH78578 was assessed by determining MIC and MBC in mLB medium. Here, approximately 3×10^7 CFU mL^{-1} log phase bacterial cells were exposed to different concentrations of L-Ag NPs [0.5-64 µg (Ag) mL^{-1}] following published protocols (30, 31). The MIC of the L-Ag NPs was determined to be 21 µg (Ag) mL^{-1} (Figure 2B). To further determine the bactericidal efficiency of L-Ag NPs, *K. pneumoniae* MGH78578 exposed to different concentrations of L-Ag NPs were spread plated and incubated for 12 h at 37 °C. The concentration

of L-Ag NPs with no visible bacterial growth was recorded as the MBC and this value was 45 µg (Ag) mL^{-1} (Figure S2).

Biochemical analysis shows the generation of ROS, membrane damage and intracellular uptake of Ag^+

Silver nanoparticles can dissolve and release Ag^+ into the surrounding medium, exposing bacterial cells to a barrage of bactericidal Ag^+. However, the dissolution kinetics of L-Ag NPs depends on their physicochemical properties (26). We measured the amount of released Ag^+ following incubation of L-Ag NPs in mLB from 2 to 8 h at 37°C (Figure 2C). Limited dissolution was observed, though a significant time-dependent increase in the concentration of Ag^+ was noted, suggesting the release of Ag^+ from L-Ag NPs under our experimental conditions. Fresh L-Ag NP suspensions were used for all the microbiological experiments.

We determined the concentration of silver that enter *K. pneumoniae* MGH78578 following treatment with L-Ag NPs for 5, 30, and 60 min in mLB at 37°C. The bacterial cells were washed and the pellet subjected to acid digestion before analysis of the cellular silver concentration by ICP-OES. We observed that uptake of silver, either in the form of L-Ag NPs or Ag^+, is directly proportional to the time duration of treatment (Figure S3).

Both L-Ag NPs and released Ag^+ could potentially generate reactive oxygen species (ROS) outside the bacterial cells. Extracellular ROS production was evaluated by measuring the oxidative potential of L-Ag NPs in a simplified synthetic respiratory tract lining fluid (sRTLF). The depletion of antioxidants, uric acid, acetic acid, and reduced glutathione GSH, was measured by HPLC following incubation of L-Ag NPs in sRTLF for 4 h at 37 °C (32). The depletion in ascorbic acid and GSH was dose-dependent for L-Ag NP concentrations ranging from 1 to 10 µg mL^{-1} (Figure 3A). About 20% and 50% depletion in ascorbic acid and GSH respectively were induced at a concentration of 1 µg mL^{-1} L-Ag NPs. A concentration of 5 µg mL^{-1} L-Ag NPs induced full oxidation of both compounds. These results show that L-Ag NPs can lead to the generation of ROS even at low NP concentration outside the bacterial cell. To determine whether ROS are also produced inside the bacterial cells following exposure to L-Ag NPs, we used the DCFH-DA assay, which is based on the emission of a cell-permeable fluorogenic dye following oxidation. Some NPs can interact with fluorometric assays by quenching the fluorescence emission following NP internalization (33). However, no artefacts were reported in the case of silver NPs (34). Our fluorescence data show a dose-dependent increase in the ROS internal to the bacterial cell (Figure 3B), a reflection of the oxidative stress external to the bacterial cell. In short, when treated with L-Ag NPs, bacteria are exposed to severe oxidative stress.

The oxidative stress induced by L-Ag NPs could lead to many downstream phenotypes in bacteria including compromised membrane integrity, depletion in cellular energy, among others (35). Since compromised membrane integrity is a key phenotype underpinning NP exposure (26, 36), we focused on the characterization of the membrane integrity in L-Ag NP exposed *K. pneumoniae*. TEM analysis of a minimum of 50 cells did not show any change in the membrane integrity of the bacterial cell when compared to the control (Figures 3C-D). To confirm our TEM observation, we explored the degree of bacterial membrane damage in the whole population using an MDA assay, which measures the lipid peroxidation of the bacterial membrane. We noted a limited though significant concentration-dependent increase in the level of lipid peroxidation (Figure 3E). To further confirm this result we used an additional protocol, the anthrone assay, which measures the content of intracellular carbohydrate released due to the membrane damage. Similar to the MDA assay, a concentration-dependent increase was observed for carbohydrate released outside the cell due to membrane damage induced by L-Ag NP exposure (Figure 3F). Overall, our results show that L-Ag NPs induced limited bacterial membrane damage, a phenotype that was not observed by TEM.

L-Ag NP exposure induces an oxidative stress response in *K. pneumoniae* MGH78578

Since a significant anti-*Klebsiella* activity was recorded during exposure to L-Ag NPs (Figure 2B), it was of interest to understand the mechanism of antibacterial action. We used RNA-seq to understand how *K. pneumoniae* MGH78578 responded to L-Ag NP exposure. Previously we deployed RNA-seq to deduce the transcriptome of *K. pneumoniae* MGH78578 when exposed to sub-inhibitory concentrations of a chemosensitizer (37). Technical limitations of the RNA-seq experiment necessitated that the bacteria be exposed to L-Ag NPs and yet be viable for quality RNA isolation. So we exposed *K. pneumoniae* MGH78578 to a sub-inhibitory concentration of L-Ag NPs at 75% of MIC which is reflected by a concentration of 15.8 µg (Ag) mL^{-1}, thereafter denoted as MIC_{75}, before RNA isolation and subsequent sequencing (see Materials and Methods).

Klebsiella pneumoniae MGH78578 was treated with MIC_{75} L-Ag NPs for a period of 5- and 30-min. The 5 min time point was used to identify the transcriptional signals associated with *early exposure*, whilst the 30 min time point demonstrated the *adaptive responses* of L-Ag NP exposed *K. pneumoniae* (the replication time of *K. pneumoniae* MGH78578 is 20 min). Untreated bacteria were used as control. RNA was isolated from both exposed/control bacteria and deep-level sequencing was carried out. Approximately 336 million reads were obtained across all 8 libraries with an average of 42 million reads *per* library (Table S1), sufficient for downstream transcriptomic analysis (37, 38). The *VOOM* function in the *limma* package (39) was used to identify those *K. pneumoniae* MGH78578 genes that are differentially regulated. Only those found to be statistically significant (False Discovery Rate value at $p \leq 0.05$ (adjacent *p value*)) (37), were selected for further analysis. We obtained statistically significant data for a total of 3,760 and 3,945 genes following 5 min and

30 min exposure respectively (Figure 4A) (Supplementary dataset WS1). From this list of statistically significant genes, those with a $\log_2$ fold change expression of ≥ 1.0 and ≤ -1.0 (exposed *versus* unexposed cells) were considered to be up- and downregulated respectively (37, 40). For the post-5 min exposure, 1,008 genes were found to be upregulated and 1,063 genes were downregulated. Of the remaining 1,689 genes, the $\log_2$ fold change of expression was calculated to be between 1.0 and -1.0, and so were designated as having no change in expression. Similarly, at 30 min post exposure, 1,205 genes were found to be upregulated and 1,246 genes were downregulated (Figure 4B). Among all the upregulated genes at the 5- and 30-min post L-Ag NP exposure, 705 genes were found to be commonly upregulated whereas, 303 and 500 genes were uniquely upregulated during treatments at 5 min and 30 min respectively. For downregulated genes, 810 genes were found to be commonly downregulated at both time points whereas 253 and 436 genes were specifically downregulated in 5 min and 30 min treatment (Figure 4C).

The validation of our transcriptomic dataset was carried out using qRT-PCR on selected genes that were found to be differentially regulated in the RNA-seq dataset. We selected representative genes related to bacterial defence system (*soxS*), transcriptional regulator (*ramA*), outer membrane porin proteins (*ompC*) and virulence (*rfaH*). Gene expression was analyzed by $2^{-\Delta\Delta Ct}$ method. Gene expression analysis by qRT-PCR reflected a similar pattern of results when compared to RNA-seq data, supporting the strength of our transcriptional analysis, and increased confidence in these RNA-seq datasets (Supplementary Figure S4).

An earlier publication used microarray technology to characterize the transcriptome of Ag NP exposed *E. coli* (41). A comparison of our RNA-seq dataset with this published *E. coli* transcriptome dataset showed that, of the 51 *E. coli* genes belonging to different functional groups, 42 *K. pneumoniae* MGH78578 genes showed similar expression patterns, further confirming the robustness of our gene expression dataset. This comparison also highlighted the universal response of bacteria when exposed to Ag NPs. However, experimental data from more bacterial genera are needed to support this observation, at this time.

Earlier experiments demonstrated that L-Ag NPs and/or released Ag^+ resulted in the generation of ROS outside the bacterial cell, thereby exposing *K. pneumoniae* MGH78578 to stress. The transport of Ag^+ into the bacterial cell also generates intracellular ROS. Consequently, the oxidative stress responses in the bacterial cell are activated. Our RNA-seq data shows that this oxidative stress response is choreographed by both *soxS* and *oxyR,* two major transcriptional factors that respond to oxidative stress in *Enterobacteriaceae* (42). The OxyR system functions as a global regulator of peroxide stress whilst the SoxRS system is involved in the control of superoxide stress (42, 43). Increased intracellular ROS levels induce the oxidation of OxyR protein, which in turn activates detoxifying processes including heme biosynthesis, thiol-disulphide isomerization, among

others (44). In the case of the SoxRS regulon, oxidative stress causes the oxidization of the SoxR protein, which activates the *soxS* transcriptional regulator, thereby triggering a bacterial defence mechanism involving various efflux pumps and redox counter measures (42). In L-Ag NP exposed *K. pneumoniae* MGH78578, *soxS* was highly upregulated (300-fold in 5 min and 88-fold in 30 min) and *oxyR* was moderately upregulated (approximately 5-fold in both time points) (Supplementary dataset WS1). This suggested that the oxidative stress regulon was active throughout the 30 min of L-Ag NP exposure time, particularly for the *soxS* regulon.

To confirm this, we compared our RNA-seq dataset to the *K. pneumoniae* MGH78578 oxidative *soxS* regulon generated earlier (45). We found that of the 254 genes belonging to the oxidative *soxS* regulon, 129 (~51%) had similar expression patterns in both datasets, confirming that the *soxS* regulon is activated in L-Ag NP exposed *K. pneumoniae* (Supplementary dataset WS2). A typical example of *soxS* induction can be visualized in the expression of *fpr* [ferredoxin-NADP$^+$ reductase], which was induced at 22-fold at 5 min and 9-fold at 30 min post-exposure to L-Ag NPs. In response to *soxS* activation, a redox neutralization process is triggered related to the overexpression of *fpr* by 4.5-fold at 5 min that then reduced to 3.2-fold at 30 min post-treatment (46).

Bacteria activate various efflux pumps in response to intracellular Ag^+, primarily to expel the toxic Ag^+ (47). Our RNA-seq data confirms this observation. Classic efflux pump genes such as *acrAB-tolC* (48, 49) and *marRAB* were found to be highly upregulated, a feature that was sustained throughout the tested period of 30 min, possibly driven by the positive regulation *via* SoxS (42, 45). Another efflux pump encoded by the *silCFBA* operon conferring a silver resistance phenotype was also upregulated. Transcription of the *silCFBA* operon and *silP* are controlled by the *silRS*, which encodes a two-component system wherein SilR acts as a response regulator and SilS acts as a histidine kinase (50, 51). SilP is a P-type ATPase efflux pump, which facilitates the passage of Ag^+ from cytoplasm to the periplasm. SilF acts as a chaperone and transfers the silver from periplasm to the SilCBA complex, which is a three-protein dependent cation/proton antiporter system. Another protein from silver resistance system is SilE, present downstream to the *silRS* (50, 51) (Figure 5). Upregulation of *silC/B/E/R/S/P* and KPN_pKPN3p05946 genes were noted in our RNA-seq data showing the activation of efflux pumps, encoding a possible silver resistance in response to L-Ag NP exposure (Supplementary dataset WS1).

L-Ag NPs elicit the inhibition of type II fatty acid biosynthesis in *K. pneumoniae* MGH78578

K. pneumoniae MGH78578 is a multi-drug resistant strain (52). L-Ag NP exposure dependent activation of *acrAB-tolC, marRAB,* and *sil* genes should, in principle, confer silver resistance in *K. pneumoniae*. Additionally, the strong oxidative stress response should enable the bacterium to counter the oxidative stress induced by L-Ag NPs. Both of these mechanisms should render *K.*

pneumoniae MGH78578 resistant against silver. However, *K. pneumoniae* MGH78578 was found to be susceptible to L-Ag NPs. We hypothesized that the bactericidal activity of L-Ag NPs could be due to a hitherto unknown mechanism, rather than the most commonly reported oxidative stress based bactericidal activity (26). To test this, we compared our RNA-seq data to the transcriptional response of *E. coli* exposed to 37 antimicrobial compounds (53). This global transcriptional profile of *E. coli* exposed to 37 antibiotics generated a list of 447 genes whose signature expression pattern characterized the mechanism of action associated with each antibiotic. These authors report that the antibacterial action mechanism of any unknown/uncharacterized compounds can be deduced by comparing the transcriptional profile of a compound of interest with that of these 447 *E. coli* MG1665 K12 genes. To understand the antibacterial action mechanism of L-Ag NPs, we compared our exposed *K. pneumoniae* MGH78578 transcriptional data set with each individual dataset obtained from *E. coli* global transcriptional profile. Our comparative analysis showed that the highest number of similarly expressed gene pairs were obtained from the triclosan exposure dataset, suggesting that exposure to L-Ag NPs induced a triclosan-like exposure response in *K. pneumoniae* MGH78578. About 76% of the gene pairs (73 of 96 genes) (Supplementary dataset WS3 and WS4) at 5 min L-Ag NP exposure and about 74.4% (87 of 117 genes) (Supplementary dataset WS5 and WS6) at 30 min exposure had similar expression patterns compared with the *E. coli* triclosan dataset.

Further experiments were carried out to explore the mechanism underpinning the triclosan-like antibacterial activity. Triclosan is a broad-spectrum antimicrobial compound that acts by inhibiting FabI (a NADH-dependent enoylacyl carrier), a protein belonging to the type II fatty acid biosynthesis, part of a well-conserved pathway that is essential for bacterial survival. Inhibition of fatty acid biosynthesis compromises the bacterial cell membrane. During exposure to L-Ag NPs, some *K. pneumoniae* MGH78578 genes associated with type II fatty acid biosynthesis including *fabA/H/D/G/F/B* were significantly downregulated particularly during the adaptive response at 30 min (Supplementary dataset WS1). The downregulation of the different *fab* genes signals a compromised type II fatty acid biosynthesis underpinning the triclosan-like L-Ag NP bactericidal activity.

Importantly, *fadL* and *fadD* were downregulated. FadL is a porin that is used to transport extracellular fatty acids across the outer membrane to the inner membrane where they are activated by acyl CoA synthetase FadD. Downregulation of both *fadL* and *fadD* shows that extracellular fatty acids are not transported leading to subsequent suppression of type II fatty acid biosynthesis pathway. We, however, did not observe any differential expression in the *fabI* gene, possibly because the triclosan affects FabI post translationally.

Recently, the TraDIS-Xpress approach involving a transposon mutant library and massively parallel sequencing of transposon chromosome junctions was used to identify *E. coli* genes that respond to triclosan exposure (54). In comparison, we identified genes that were both enriched in the *E. coli* TraDIS-Xpress dataset and that were also found to be differentially expressed in the *K. pneumoniae* MGH78578 dataset. Common genes like *purL, purH, waeL, wzx* were downregulated at either one or both time points while *metB* was upregulated. Similarly, *K. pneumoniae* MGH78578 genes like *trkA, pcnB, infB,* and *ubiB/F*, whose *E. coli* mutants were selected in the TraDIS-Xpress based triclosan exposure assay, were downregulated at least in one or both time points, while *lonH* was upregulated (Supplementary dataset WS1). TraDIS-Xpress selected *rbs* in their triclosan exposure screen. In *E. coli,* RbsABC forms the ABC-type high-affinity D-ribose transporter, while RbsD/K converts D-ribose into D-ribose 5-phosphate (55). Though we did not observe a statistically significant differential expression for *rbsB,* down-regulation was observed for *rbsD* and *rbsC,* showing compromised D-ribose uptake. Similar observations across different datasets gave confidence to our earlier observation that L-Ag NP exposure elicits a *triclosan like* bactericidal effect in *K. pneumoniae* inhibiting type II fatty acid biosynthesis.

Finally, we investigated whether the L-Ag NP based antibacterial effect was primarily due to type II fatty acid biosynthesis inhibition or as a cumulative effect of both oxidative stress and type II fatty acid biosynthesis inhibition. For this, we exposed the isogenic *K. pneumoniae MGH78578 ΔsoxS* mutant to L-Ag NPs and measured the MIC. The *K. pneumoniae ΔsoxS* mutant has a compromised oxidative stress response mechanism (45). The MIC of L-Ag NPs further reduced to 15 µg mL^{-1} as opposed to 21 µg mL^{-1} as measured for the wild type *K. pneumoniae* MGH78578, showing that oxidative stress did contribute to a significant antibacterial effect. Therefore, we deduce that the antibacterial effect of L-Ag NPs is a cumulative effect of both type II fatty acid biosynthesis inhibition and oxidative stress responses. The role of genes involved in mRNA protection, protein stability, might also be important, though more confirmatory experiments are needed to validate our observation.

Potential mechanisms of resistance against L-Ag NPs in *K. pneumoniae*

We observed that L-Ag NPs are very efficient in killing multi drug-resistant *K. pneumoniae* MGH78578. They trigger a *triclosan-like* mechanism to exert their anti-*Klebsiella* effect. We propose that, with toxicity studies in appropriate cell lines/models, L-Ag NPs may be a future candidate as a novel antimicrobial agent. If so, there is also a possibility that bacteria can generate antimicrobial resistance against L-Ag NPs. We hypothesized that our RNA-seq data could provide clues as to how *K. pneumoniae* might develop resistance. A closer examination of the expression pattern of some of the earlier genes mentioned above, particularly *rbsD/C, trkA, pcnB* and *infB,* enabled us to formulate a hypothesis. The above five genes were downregulated during adaptive

response at 30 min in the exposed L-Ag NP dataset (Supplementary dataset WS1). Transposon insertional mutants of *E. coli* genes *trkA, pcnB* and *infB* exhibit better survival in the presence of triclosan (54). Transposon insertion in *rbsB,* inhibiting the periplasmic ribose-binding domain of the RbsABC ribose importer, also gave a selective survival advantage in the presence of triclosan. Therefore, we hypothesize that by downregulating these genes during the adaptive response, *K. pneumoniae* MGH78578 could elicit strategies to combat and develop resistance against L-Ag NPs.

It should also be noted that the RNAseq experiment was carried out at MIC_{75}, wherein the bacterium was exposed to sub-inhibitory concentrations of L-Ag NPs. Exposure to sub-inhibitory concentrations of antimicrobial compounds is one of the main drivers in the evolution of antibiotic resistance. By continuous exposure to sub-inhibitory concentrations of silver and the subsequent downregulation of the above-discussed genes, *K. pneumoniae* might offer a transient resistance to L-Ag NPs. This hysteresis effect might be the prelude to developing a fully expressed antimicrobial resistance mechanism against silver.

Materials and Methods

Materials. All chemicals used in this study for antibacterial susceptibility testing were of analytical grade and were purchased from Sigma Aldrich (USA) unless otherwise stated. Oligonucleotide primers were synthesized commercially by Integrated DNA Technologies Inc. Milli-Q water was acquired from a Milli-Q Biocel water purification system manufactured by Merck Millipore (Merck KGaA, Darmstadt, Germany).

Synthesis and characterization of lysozyme-coated silver nanoparticles. L-Ag NPs were synthesized following a protocol reported earlier by Ashraf et al. (18). Our protocol is described in detail in Supplementary information. To determine the size, shape, charge, crystallinity and surface capping, L-Ag NPs were characterized by Transmission Electron Microscopy combined with Energy Dispersive Spectroscopy (TEM-EDS), X-ray Diffraction (XRD), UV-vis spectroscopy, and Fourier Transform Infrared spectroscopy (FTIR). The zeta potential of L-Ag NPs was measured in water and in modified LB medium with a Zetasizer Nano ZS (Malvern Instruments). All experiments were performed in duplicate. Each method is described in detail the Supplementary information. The acellular oxidative potential of L-Ag NPs was assessed by measuring the depletion in antioxidants, uric acid, ascorbic acid, and reduced glutathione, following incubation of L-Ag NPs at a concentration of 1 to 10 µg mL^{-1} in a simplified synthetic respiratory tract lining fluid (sRTLF) for 4 h at 37 °C. sRTLF composed of 200 µM uric acid (UA), 200 µM ascorbic acid (AA) and 200 µM reduced glutathione (GSH) in 9 g L^{-1} NaCl at pH 7.4 was prepared following guidelines (56). Then these solutions were centrifuged on SpinX 0.2 µm cellulose acetate filters at 12,000 g and the antioxidant (UA, AA, GSH) and oxidized glutathione (GSSG) concentrations were measured by reverse-phase HPLC. A sample containing sRTLF only was used as a reference. The depletion in

reduced glutathione was confirmed by the formation of oxidized glutathione (GSSG). The depletion in antioxidant was expressed as the ratio between the antioxidant concentration difference between the reference and the sample, divided by the antioxidant concentration of the reference. All measurements were performed in duplicates. The results are expressed as mean ± standard deviation. The detailed protocol for the assay is described in the Supplementary information.

Cultivation of bacterial and physiological analysis of L-Ag NP antibacterial potential. *Klebsiella pneumoniae* MGH78578 (ATCC®700721) was procured from the American Type Culture Collection, USA. This bacterium is a clinical isolate, originally cultured in 1994, from a 66-year-old ICU patient. This strain was chosen because of its multidrug resistant phenotype (37, 57). The main advantage behind the selection of this strain was the availability of its whole genome sequence (Reference Sequence NC_009648.1). Detailed methodology for the preparation of bacterial culture is provided in Supplementary information. Considering previous reports describing precipitation of Ag^+ with Cl^- in Luria Bertani (LB) bacterial culture media (casein enzyme hydrolysate 10 g L^{-1}, yeast extract 5 g L^{-1}, NaCl 10 g L^{-1}, pH 7.2 ± 0.2) (19, 29) , bacterial growth was compared in LB and modified LB (mLB) media (constituted without NaCl). An overnight grown bacterial culture (approximately 10^7 CFU mL^{-1}) was inoculated separately in freshly prepared LB and mLB broth medium (casein enzyme hydrolysate 10 g L^{-1}, yeast extract 5 g L^{-1}, pH 7.2 ± 0.2). Bacterial growth was determined by measuring the optical density (OD) at 600 nm against a blank (no bacterial cell) at 2 h time intervals. All experiments were performed in both technical and biological duplicates and the results are represented as mean ± standard deviation. A minimum inhibitory concentration (MIC) assay, using broth microdilution following standard guidelines Clinical and Laboratory Standards Institute (CLSI) (58) was performed to determine the lowest concentration of L-Ag NPs required to inhibit the growth of *K. pneumoniae* MGH78578. To analyse the MBC (minimum bactericidal concentration) of L-Ag NPs, bacterial cells were again exposed to the broad concentration range of L-Ag NPs (0.5 to 64 µg (Ag) mL^{-1}) and incubated at 37 °C in the dark for 24 h. Complete methodology for the analysis of MIC and MBC is discussed in the Supplementary information. Freshly prepared L-Ag NPs were used for all the experiments.

Biochemical analysis of antibacterial mechanism. The dissolution kinetics of L-Ag NPs was measured in mLB at 37 °C under constant agitation, using an initial concentration of 10 µg (Ag) mL^{-1} L-Ag NPs in 10 mL mLB medium. The concentration of Ag^+ was measured at 2, 4, 6, 8 h by inductively coupled plasma optical emission spectrometry (ICP-OES) (Avio 200, PerkinElmer, USA). The experiments were performed in duplicate. To measure the generation of ROS inside the bacterial cell following exposure to L-Ag NPs, a 2,7-dichlorodihydrofluorescein diacetate (DCFH-DA) assay was performed with minor modifications of the original protocol of Wang and Joseph (59). The complete protocol for the assay is described in the Supplementary information. The effect of L-Ag NPs on the bacterial cell envelope was examined by analyzing the treated bacterial cells

by Transmission Electron Microscopy (TEM). A minimum number of 50 bacterial cells were observed on different TEM images in each condition. The extent of damage to the bacterial cell was analyzed in terms of lipid peroxidation using a malondialdehyde (MDA) assay, and the measurement of released carbohydrate from cell cytoplasm to the exterior by the anthrone assay. Detailed methodology for the sample preparation for TEM, MDA assay and anthrone assay is presented in the Supplementary information. All the experiments were performed in duplicates. The intracellular concentration of silver in L-Ag NP treated cells was measured by ICP-OES following exposure to MIC_{75} L-Ag NPs for 5, 30 and 60 min. at 37 °C and acidic digestion of bacterial cells in HNO_3:H_2O_2 mixture. The protocol is further described in the Supplementary information.

RNA sequencing (RNA-seq) and quantitative real-time polymerase chain reaction (qRT-PCR). For RNA-seq, a freshly grown culture of *K. pneumoniae* MGH78578 from mid-log_{10} phase (approximately 10^7 CFU mL^{-1}) was exposed to MIC_{75} L-Ag NPs for 5 and 30 min at 37 °C in mLB broth, separately. The time and concentration of L-Ag NP treatment was selected based on the results obtained in the biochemical analysis. Bacterial cells not exposed to L-Ag NPs were selected as a control for each time point. After exposure to L-Ag NPs, RNA was isolated from the bacterial pellet using RNAeasy extraction kit (Qiagen, Hilden, Germany) following manufacturer's instructions. To remove any DNA contamination, the isolated RNA was treated with Turbo DNase kit (Ambion's, USA). The integrity of the DNase treated RNA was assessed using a Bioanalyzer 2100 RNA 6000 nanochip (Agilent Technologies, United States). Purified RNA was then carefully stored at -80°C until further use. RNA library preparation and subsequent sequencing was performed commercially at the Centre for Genomic Research, University of Liverpool, UK. In total 8 libraries were prepared as outlined in Table S1. For the removal of ribosomal RNA, a Ribo-Zero rRNA removal kit (Illumina, USA) was used according to the manufacturer's instructions. For the preparation of libraries from purified RNA sample, NEBNext® Directional RNA Library Prep Kit (New England BioLabs, Germany) was used. Pooled libraries were loaded on cBot (Illumina) and cluster generations was performed as per the manufacturer's instructions. Single- sequencing using 150 bp read length was performed on lane of the HiSeq 4000 sequencer (Illumina). Raw sequencing data were processed and validated as discussed in Supplementary information. The RNAseq data produced from the present work was deposited to the NCBI-GEO database and are available under the accession number GSE151953.

Deduction of the antibacterial action mechanism of L-Ag NPs from the gene expression patterns in the RNA-seq dataset. A manual comparison of our transcriptional data with the global transcriptome profiling of *E. coli* MGH1665 K12 strain exposed to 37 antibiotics was carried out. Only those genes that gave statistically significant differential expression patterns were selected from both datasets. Our gene expression dataset was compared to each of the 37 *E. coli*

transcriptional profiles and genes that had similar expression patterns (both up-and downregulation) were counted.

Acknowledgments

Authors are thankful to BITS Pilani, University College Dublin, and Université de Paris for providing lab facilities. VP acknowledges CSIR-SRF [09/719(0090)/2018-EMR-l] and EMBO Short Term Fellowship (ESTF 7654) for the financial support. We acknowledge Justine Renault, Linh-Chi Bui, and the Bioprofiler Facility (BFA) for the HPLC analysis. This project was supported, in part, by the Ulysses PHC Scheme.

Author Contributions

SD, SS, SF, JP designed the study. VP, AB, SD characterized the silver NPs. VP and SS carried out the RNA-seq experiments. SKS generated the bioinformatics based gene expression dataset. SS, SD, VP, SF carried out the detailed RNA-seq dataset analysis that led to the triclosan observation. All authors read and approved the manuscript.

Competing Interest Statement

The authors declare no competing interests.

References

1. M. J. Baker et al., Using Fourier transform IR spectroscopy to analyze biological materials. *Nat. Protoc.* 9, 1771 (2014).
2. World Health Organization. No time to wait: securing the future from drug-resistant infections. Report to the Secretary-General of the United Nations. World Health Organization, Geneva (2019).
3. J. N. Pendleton, S. P. Gorman, B. F. Gilmore, Clinical relevance of the ESKAPE pathogens. *Expert Rev. Anti. Infect. Ther.* 11, 297-308 (2013).
4. E. J. Klemm, V. K. Wong, G. Dougan, Emergence of dominant multidrug-resistant bacterial clades: Lessons from history and whole-genome sequencing. *Proc. Natl. Acad. Sci. U.S.A.* 115, 12872-12877 (2018).
5. R. Podschun, U. Ullmann, *Klebsiella spp.* as nosocomial pathogens: epidemiology, taxonomy, typing methods, and pathogenicity factors. *Clin. Microbiol. Rev.* 11, 589-603 (1998).
6. G. C. Lee, D. S. Burgess, Treatment of *Klebsiella pneumoniae* carbapenemase (KPC) infections: a review of published case series and case reports. *Ann. Clin. Microbiol. Antimicrob.* 11, 32 (2012).
7. J. Jagnow, S. Clegg, *Klebsiella pneumoniae MrkD*-mediated biofilm formation on extracellular matrix-and collagen-coated surfaces. *Microbiology* 149, 2397-2405 (2003).
8. B. Li et al., Molecular pathogenesis of *Klebsiella pneumoniae*. *Future Microbiol.* 9, 1071-1081 (2014).
9. Y. Hu et al., *Klebsiella pneumoniae*: prevalence, reservoirs, antimicrobial resistance, pathogenicity and infection: a hitherto unrecognised zoonotic bacterium, *Foodborne Pathog. Dis.* (*in press*).
10. J. H. Han et al., Epidemiology of carbapenem-resistant *Klebsiella pneumoniae* in a network of long-term acute care hospitals. *Clin. Infect. Dis.* 64, 839-844 (2016).

11. A. Antoniadou *et al.*, Colistin-resistant isolates of *Klebsiella pneumoniae* emerging in intensive care unit patients: First report of a multiclonal cluster. *J. Antimicrob. Chemother.* 59, 786-790 (2007).
12. E. A. Neuner et al., Treatment and outcomes in carbapenem-resistant *Klebsiella pneumoniae* bloodstream infections. *Diagn. Micr. Infec. Dis.* 69, 357-362 (2011).
13. R. Adamo, I. Margarit, Fighting Antibiotic-Resistant *Klebsiella pneumoniae* with “Sweet” Immune Targets. *mBio* 9, e00874-00818 (2018).
14. J. W. Alexander, History of the medical use of silver. *Surg. Infect.* 10, 289-292 (2009).
15. K. Mijnendonckx et al., Antimicrobial silver: uses, toxicity and potential for resistance. *Biometals* 26, 609-621 (2013).
16. R. Li et al., Synergistic reaction of silver nitrate, silver nanoparticles, and methylene blue against bacteria. *Proc. Natl. Acad. Sci. U.S.A.* 113, 13612-13617 (2016).
17. S. Chernousova, M. Epple, Silver as antibacterial agent: ion, nanoparticle, and metal. *Angew. Chem. Int. Ed.* 52, 1636-1653 (2013).
18. S. Ashraf et al., Lysozyme-coated silver nanoparticles for differentiating bacterial strains on the basis of antibacterial activity. *Nanoscale Res. Lett.* 9, 565 (2014).
19. A. Bhargava et al., Superior bactericidal efficacy of fucose-functionalized silver nanoparticles against *Pseudomonas aeruginosa* PAO1 and prevention of its colonization on urinary catheters. *ACS Appl. Mater. Interfaces* 10, 29325-29337 (2018).
20. R. R. Mishra, P. Chandran, S. S. Khan, Equilibrium and kinetic studies on adsorptive removal of malachite green by the citrate-stabilized magnetite nanoparticles. *RSC Adv.* 4, 51787-51793 (2014).
21. H. R. Ibrahim et al., A structural phase of heat-denatured lysozyme with novel antimicrobial action. *J. Agric. Food Chem.* 44, 1416-1423 (1996).
22. D. M. Eby et al., Lysozyme catalyzes the formation of antimicrobial silver nanoparticles. *ACS Nano* 3, 984-994 (2009).
23. D. K. Singh et al., Mycosynthesis of bactericidal silver and polymorphic gold nanoparticles: physicochemical variation effects and mechanism. *Nanomedicine* 13, 191-207 (2018).
24. N. Jain et al., Extracellular biosynthesis and characterization of silver nanoparticles using *Aspergillus flavus* NJP08: a mechanism perspective. *Nanoscale* 3, 635-641 (2011).
25. V. Pareek, A. Bhargava, J. Panwar, Biomimetic approach for multifarious synthesis of nanoparticles using metal tolerant fungi: A mechanistic perspective. *Mater. Sci. Eng. B* 262, 114771 (2020).
26. V. Pareek, R. Gupta, J. Panwar, Do physico-chemical properties of silver nanoparticles decide their interaction with biological media and bactericidal action? A review. *Mater. Sci. Eng. C* 90, 739-749 (2018).
27. C.-N. Lok et al., Silver nanoparticles: partial oxidation and antibacterial activities. *J. Biol. Inorg. Chem.* 12, 527-534 (2007).
28. J. S. McQuillan et al., Silver nanoparticle enhanced silver ion stress response in *Escherichia coli* K12. *Nanotoxicology* 6, 857-866 (2012).
29. B. A. Chambers *et al.*, Effects of chloride and ionic strength on physical morphology, dissolution, and bacterial toxicity of silver nanoparticles. *Environ. Sci. Technol.* 48, 761-769 (2013).
30. D. A. Pelletier et al., Effects of engineered cerium oxide nanoparticles on bacterial growth and viability. *Appl. Environ. Microbiol.* 76, 7981-7989 (2010).
31. S. Chatterjee, A. Bandyopadhyay, K. Sarkar, Effect of iron oxide and gold nanoparticles on bacterial growth leading towards biological application. *J. Nanobiotechnology* 9, 34 (2011).
32. B. Crobeddu et al., Oxidative potential of particulate matter 2.5 as predictive indicator of cellular stress. *Environ. Pollut.* 230, 125-133 (2017).
33. A. Aranda *et al.*, Dichloro-dihydro-fluorescein diacetate (DCFH-DA) assay: a quantitative method for oxidative stress assessment of nanoparticle-treated cells. *Toxicol. In Vitro* 27, 954-963 (2013).

34. A. Panáček et al., Bacterial resistance to silver nanoparticles and how to overcome it. *Nat. Nanotechnol.* 13, 65-71 (2018).
35. N. Jain et al., Removal of protein capping enhances the antibacterial efficiency of biosynthesized silver nanoparticles. *PloS One* 10, e0134337 (2015).
36. H.-J. Park *et al.*, Silver-ion-mediated reactive oxygen species generation affecting bactericidal activity. *Water Res.* 43, 1027-1032 (2009).
37. J. Anes et al., Exposure to Sub-Inhibitory Concentrations of the Chemosensitizer 1-(1-Naphthylmethyl)-Piperazine Creates Membrane Destabilisation in Multi-Drug Resistant *Klebsiella pneumoniae*. *Front. Microbiol.* 10, 92 (2019).
38. B. J. Haas et al., How deep is deep enough for RNA-Seq profiling of bacterial transcriptomes? *BMC Genomics* 13, 734 (2012).
39. M. E. Ritchie et al., limma powers differential expression analyses for RNA-sequencing and microarray studies. *Nucleic Acids Res.* 43, e47-e47 (2015).
40. S. Dash et al., TGF-β2-induced EMT is dampened by inhibition of autophagy and TNF-α treatment. *Oncotarget* 9, 6433 (2018).
41. J. S. McQuillan, A. M. Shaw, Differential gene regulation in the Ag nanoparticle and Ag^+-induced silver stress response in *Escherichia coli*: a full transcriptomic profile. *Nanotoxicology* 8, 177-184 (2014).
42. S. W. Seo et al., Genome-wide reconstruction of OxyR and SoxRS transcriptional regulatory networks under oxidative stress in *Escherichia coli* K-12 MG1655. *Cell Rep.* 12, 1289-1299 (2015).
43. M. Zheng, F. Åslund, G. Storz, Activation of the OxyR transcription factor by reversible disulfide bond formation. *Science* 279, 1718-1722 (1998).
44. J. M. Dubbs, S. Mongkolsuk, Peroxide-sensing transcriptional regulators in bacteria. *J. Baceteriol.* 194, 5495-5503 (2012).
45. J. Anes et al., Analysis of the oxidative stress regulon identifies *soxS* as a genetic target for resistance reversal in multi-drug resistant *Klebsiella pneumoniae*. B*ioRxiv* (2020).
46. A. R. Krapp et al., The flavoenzyme ferredoxin (flavodoxin)-NADP (H) reductase modulates NADP (H) homeostasis during the *soxRS* response of *Escherichia coli*. *J. Bacteriol. Res.* 184, 1474-1480 (2002).
47. R. Gurbanov et al., Aspects of silver tolerance in bacteria: infrared spectral changes and epigenetic clues. *J. Biophotonics* 11, e201700252 (2018).
48. Y. Hirakata et al., Efflux pump inhibitors reduce the invasiveness of *Pseudomonas aeruginosa*. *Int. J. Antimicrob. Agents* 34, 343-346 (2009).
49. S. Baugh et al., Inhibition of multidrug efflux as a strategy to prevent biofilm formation. *J. Antimicrob. Chemother.* 69, 673-681 (2013).
50. M. Starodub, J. Trevors, Silver resistance in *Escherichia coli* R1. *J. Med. Microbiol.* 29, 101-110 (1989).
51. M. B. Massani et al., Chromosomal *Sil* system contributes to silver resistance in *E. coli* ATCC 8739. *BioMetals* 31, 1101-1114 (2018).
52. J. Anes et al., Exploring the genome and phenotype of multi-drug resistant *Klebsiella pneumoniae* of clinical origin. *Front. Microbiol.* 8, 1913 (2017).
53. A. O'Rourke et al., Mechanism-of-action classification of antibiotics by global transcriptome profiling. *Antimicrob. Agents Chemother.* 64, e01207-19 (2020).
54. M. Yasir et al., TraDIS-Xpress: a high-resolution whole-genome assay identifies novel mechanisms of triclosan action and resistance. *Genome Res.* 30, 239-249 (2020).
55. T. Shimada, A. Kori, A. Ishihama, Involvement of the ribose operon repressor *RbsR* in regulation of purine nucleotide synthesis in *Escherichia coli*. *FEMS Micro. Lett.* 344, 159-165 (2013).
56. S. Boland, A. Baeza-squiban, Acellular Antioxidant Depletion Assay. NanOxiMet (2015).
57. W. Ogawa et al., Multidrug resistance in *Klebsiella pneumoniae* MGH78578 and cloning of genes responsible for the resistance. *Biol. Pharm. Bull.* 28, 1505-1508 (2005).

58. P. A. Wayne, Clinical and Laboratory Standards Institute. Methods for dilution antimicrobial susceptibility tests for bacteria that grow aerobically; Approved standard-eleventh edition. document M07-A11. CLSI, USA (2018).
59. H. Wang, J. A. Joseph, Quantifying cellular oxidative stress by dichlorofluorescein assay using microplate reader. *Free Radic. Biol. Med.* 27, 612-616 (1999).

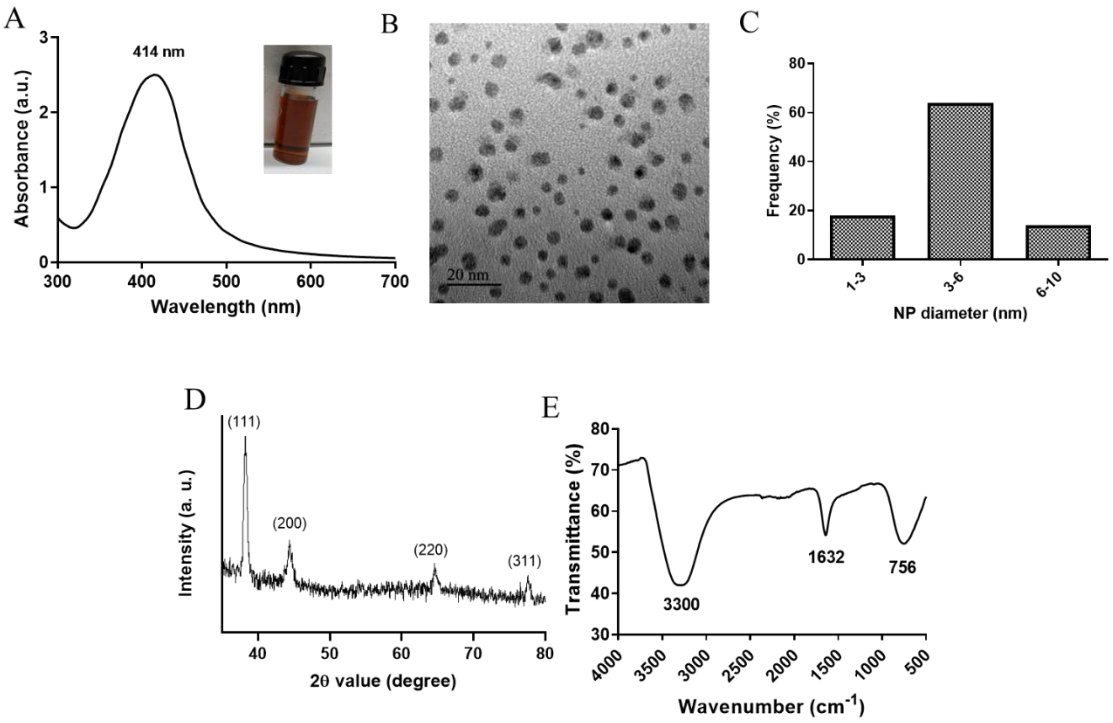

Figure 1. Characterization of L-Ag NPs. (A) UV-visible spectrum (inset shows a picture of the L-Ag NP suspension after synthesis). (B) TEM image. (C) Distribution of L-Ag NP diameter determined from TEM analysis. (D) XRD diffraction spectrum. (E) FTIR spectrum.

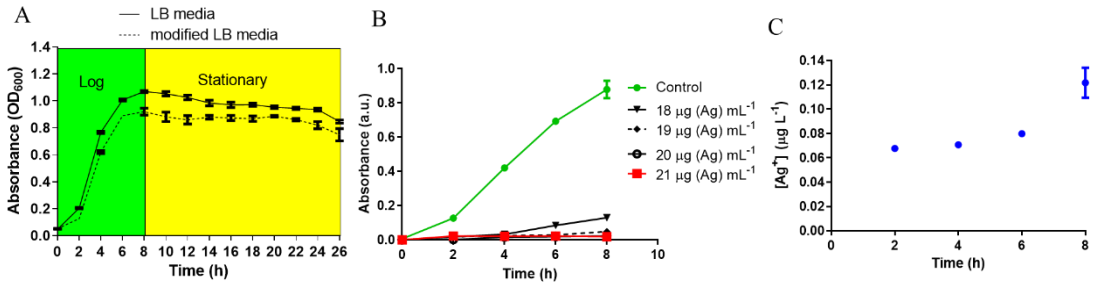

Figure 2. (A) Bacterial growth curve analysis of *K. pneumoniae* MGH78578 in LB and mLB media. (B) Determination of *K. pneumoniae* L-Ag NP MIC in mLB medium. (C) Dissolution kinetics of L-Ag NPs in mLB medium at 37°C.

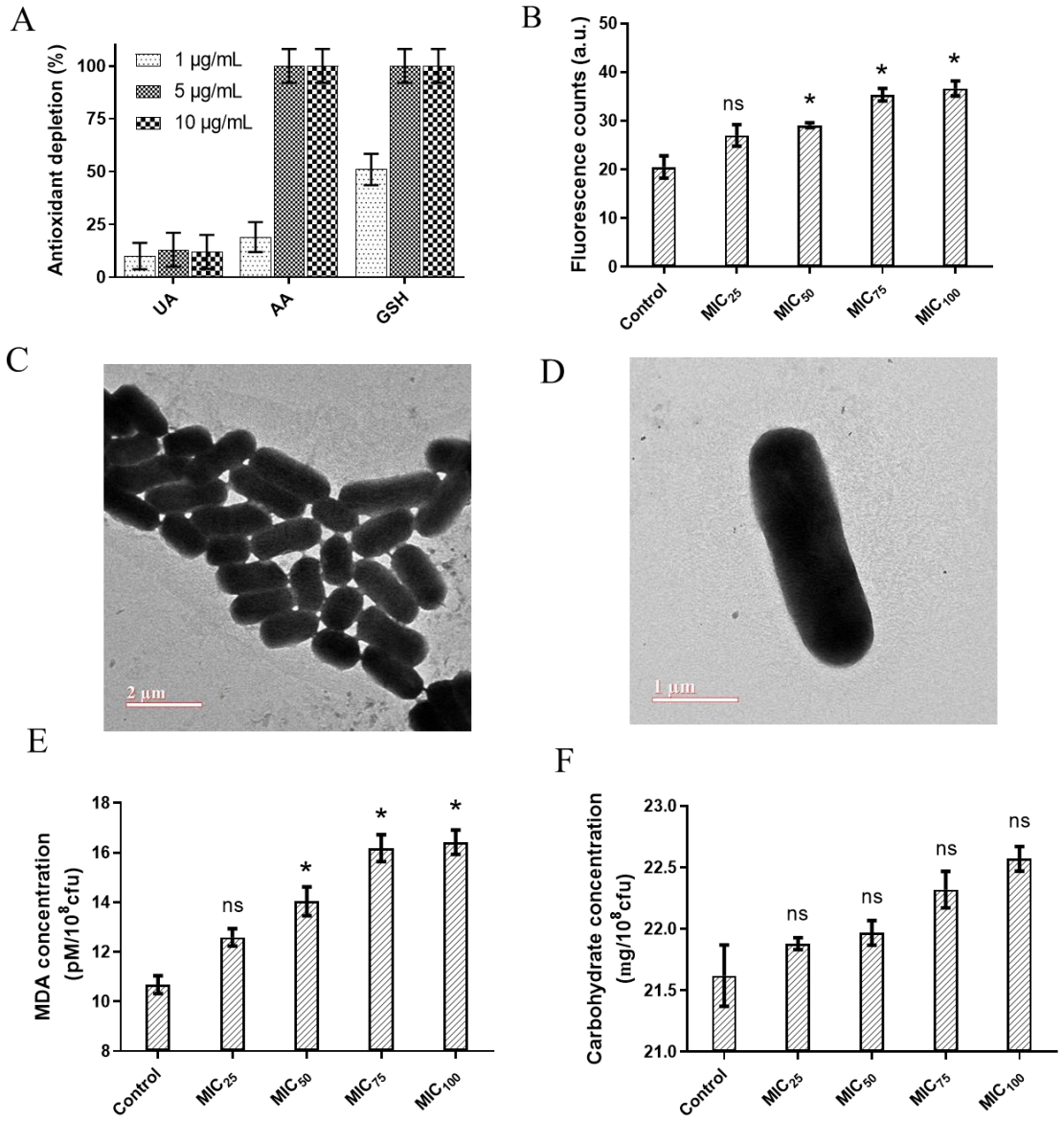

Figure 3. (A) Acellular oxidative potential of L-Ag NPs measured by the depletion of antioxidants, uric acid (UA), ascorbic acid (AA), and reduced glutathione (GSH), in simplified synthetic lung lining fluid at 37°C. (B) Analysis of the intracellular ROS generation in *K. pneumoniae* MGH78578 following exposure to L-Ag NPs by the DCFH-DA assay. (C,D) Representative TEM images of untreated *K. pneumoniae* (control) (C) and *K. pneumoniae* exposed to MIC75 of L-Ag NPs (D). (E,F) Membrane damage analysis of *K. pneumoniae* following exposure to L-Ag NPs. Analysis by MDA assay (E) and anthrone assay (F).

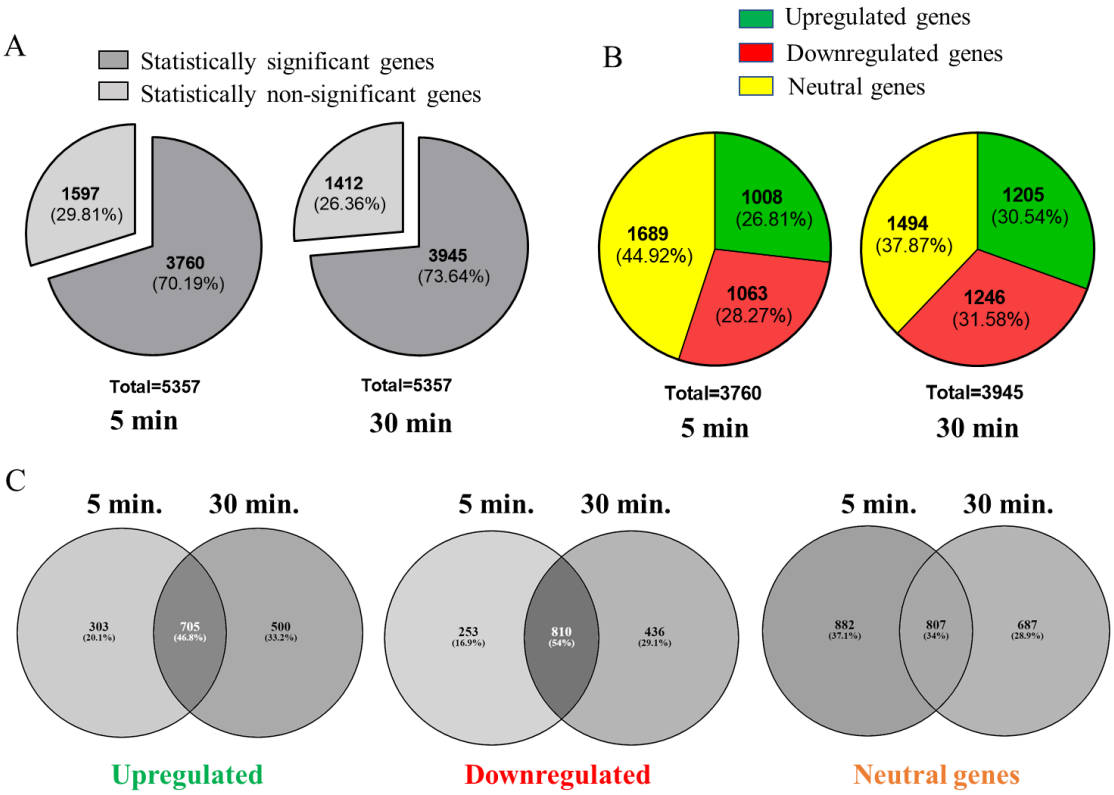

Figure 4. Overview of the RNAseq analysis of *K. pneumoniae* MGH78578 following treatment with MIC_{75} L-Ag NPs. (A) Statistically significant and insignificant genes recorded at 5 and 30 min post-treatment. (B) Statistically significant upregulated, downregulated and neutral genes identified at 5 and 30 min post-treatment. (C) Comparison of the upregulated, downregulated, and neutral genes identified at 5 and 30 min post-treatment.

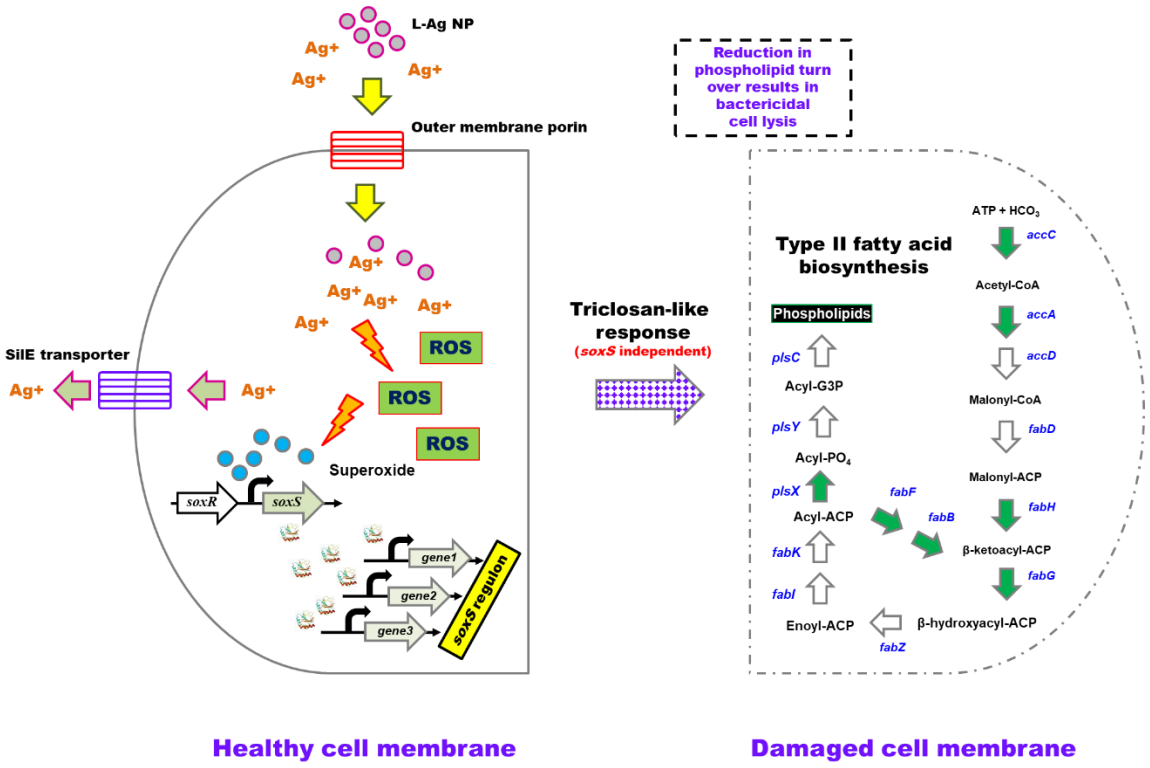

Figure 5. A model depicting the bactericidal action of L-Ag NPs on *K. pneumoniae* MGH78578. L-Ag NPs and silver ions (Ag^+) enter the bacterial cell *via* outer membrane porins. Increasing cytoplasmic Ag^+ concentration elicits the production of reactive oxygen species (ROS) including superoxide radicals, which then activate the *soxS*-mediated oxidative stress response. The SilE efflux system functions to eliminate Ag^+ from the cytoplasm. RNA-seq data identified 7 genes (denoted by the green arrowheads) associated with type II fatty acid biosynthesis that are down-regulated leading to reduced phospholipid biosynthesis. This reduction in phospholipid turnover will affect the membrane stability leading to cell lysis underpinning the bactericidal activity. Grey arrows represent genes that are activated. White arrows represent genes that are either not identified in the *K. pneumoniae* MGH78578 genome or not differentially regulated when the bacteria are exposed to L-Ag NPs.